Cardiac Cellular Coupling and the Spread of Early Instabilities in Intracellular Ca^{2+}

Zhiheng Jia,[†] Harold Bien,[†] Yohannes Shiferaw,[§] and Emilia Entcheva[†‡]

[†]Department of Biomedical Engineering and [‡]Department of Physiology and Biophysics, Stony Brook University, Stony Brook, New York; and [§]Department of Physics and Astronomy, California State University Northridge, Northridge, California

Supplementary Detailed Methods

Cardiac syncytium *in vitro*

Primary cardiac cell culture was prepared as follows[1-5]: The ventricles of the hearts of 3-day-old Sprague-Dawley rats were minced into small fragments and placed in Hanks' balanced salt solution (GIBCO Invitrogen, Carlsbad, CA). Enzymatic digestion was applied using trypsin (1 mg/ml, 4°C overnight; US Biochemicals, Cleveland, OH) and then collagenase (1 mg/ml, 37°C; Worthington Biomedical, Lakewood, NJ). After centrifugation, the supernatant was discarded and the cells were resuspended in culture medium consisting of medium 199 (GIBCO), 12 μM L-glutamine (GIBCO), 0.05 μg/ml penicillin-streptomycin (Mediatech Cellgro, Kansas City, MO), 0.2 μg/ml vitamin B12 (Sigma, St. Louis, MO), 10 mM HEPES (GIBCO), and 3.5 mg/ml D-(+)-glucose (Sigma) supplemented with 10% fetal bovine serum (GIBCO). Two-step preplating for a total of 90 min was used to eliminate fibroblasts from the cell population. The cardiomyocytes were then seeded on fibronectin-coated surfaces (50 μg/ml; BD Biosciences, Franklin Lakes, NJ) at a high density (0.4 x 106 cells/cm2) and kept at 37°C in 5% CO2 in culture medium with 10% serum on days 1 and 2 and then switched to culture medium with 2% serum changed every other day. Cells formed syncytial structures, confirmed by macroscopic mapping of electrical propagation

Scaffolds for cell growth were prepared from an elastomer, polydimethylsiloxane (PDMS; Sylgard 184, Dow Corning, Midland, MI), at 1:10 curing agent-to-monomer ratio and baked for 2 h at 60°C. The polymer was molded using metal templates.

Perturbation of cell-cell coupling and Na^+ ion channels

Reduction in cellular coupling was done by acute treatment with very low doses of heptanol (Purity>97%, Sigma-Aldrich, St. Louis, MO). As heptanol is highly volatile, it was prepared immediately before experiments and stored in capped beakers. Heptanol was diluted in Tyrode's solution to 0.25mM and 0.50mM, and at each concentration samples were perused for 10 minutes before taking measurements; in some cases washout was applied to reverse the effects.

Increase in cellular coupling was done by a small molecule, 4-phenylbutyrate (4PB), which we recently found to act as gap junction agonist[6]. 4PB (Calbiochem, La Jolla, CA) was diluted in distilled water at 500mM and stored at -20^{o}C. Chronic treatment with 4PB was applied prior to experiments: 4PB was further diluted in culture medium to final concentration of 1mM and cells were incubated at 37^{o}C for 48 hours. We have found that these treatment conditions result in upregulation in Connexin 43.

In a subset of samples (n=4), we tested the effect of sodium channel blocker TTX on wave propagation by applying TTX at concentrations: 0, 0.93, 2.8 and 8.33 μM, and measuring changes in conduction velocity during pacing at 1Hz. Mean values are shown in **Suppl. Fig. 1.**

Quantification of cell-cell coupling using fluorescence recovery after photobleaching (FRAP)

Cardiomyocyte monolayers were stained with a low molecular weight dye - calcein-AM (Invitrogen, Carlsbad, CA) at 0.5 μM for 20 min. Quantification of diffusion properties at the multicellular level was done by a macroscale version of FRAP[7]. FRAP measurements were done using Olympus confocal system with its FluoView FV1000 software package. A single cell within the field of view was selected by a free-shape polygonal drawing tool, and bleaching was carried out at 100% laser power for 1 second, followed by measurements of recovery at 1% laser power (488nm), acquiring data every 1s for at least 120s.

A complete theoretical treatment of this problem is discussed elsewhere[8, 9], and involves solving the classic diffusion equation for the concentration of the low-molecular weight fluorophore over space and time, C(r,t), if only (isotropic) lateral diffusion from the neighbors is considered:

$$\frac{\partial C(r,t)}{dt} = D\nabla^2 \mathrm{C(r,t)}, \qquad (1)$$

the boundary condition is as follows:

$$\mathrm{C}(\infty,\mathrm{t})=\mathrm{C_o}, \qquad (2)$$

and the initial condition depends on the bleaching profile, e.g. for uniformly bleached circle and first-order reaction for the fluorophore:

$$\mathrm{C(r,0) = C_o \exp[-k\Delta t\, I(r)]}, \qquad (3)$$

where Δt is the duration of the bleaching pulse, I(r) is the intensity of the pulse, and k is a rate constant related to the photobleaching process. Under these conditions, the closed-form solution of Eqn (1) for the fluorescence recovery of the bleached area via diffusion of fluorophore from the neighboring regions involves modified Bessel functions[9].

Alternatively, a simpler empirical approach can be used - fitting the experimental data to a “perturbation-relaxation” equation[7, 8] that captures in a generic way the fluorophore transport from the neighboring cells:

$$F(t) = F_0 + (F_\infty - F_0)(1 - e^{-t/\tau}) \qquad (4)$$

$F(t)$ is the normalized fluorescence intensity at time t; F_0 and F_∞ are the normalized fluorescence intensities at t=0 and ∞; τ is the time constant of recovery. While the exact (calibrated) diffusion coefficient will then depend on the specific shape of the bleached region and on the light intensity profile (Gaussian or uniform or other)[8], in all cases the diffusion coefficient will be some inverse function of the extracted time constant of recovery from Eqn (4).

To carry out the analysis, digitized fluorescence images were saved for off-line analysis using Matlab (MathWorks, Natick, MA). For each time point, the average intensity value of the cell of interest was divided by the mean intensity value of a reference cell at the edge of the field of view. Since the reference cell was unaffected by the laser bleaching, the ratios would correct

for actual changes in fluorescence intensity due to photobleaching of the entire field of view. Then the ratios were normalized to a 0-100 scale for generating normalized fluorescence recovery curves as per Eqn (4).

Experimental measurements of V_m-Ca^{2+} coupling

In a subset of samples (n=16), cells were co-stained for transmembrane voltage and intracellular calcium with di-8 ANEPPS and fura-2 AM (Molecular Probes, Eugene, OR), respectively. Cells were stimulated with a Pt line electrode at one end of the scaffold, initiating a planar wave. Cells were paced at several frequencies following a dynamic restitution protocol - frequency was varied from 1Hz to 2Hz in 0.5Hz steps and thereafter in 0.2Hz increments. Measurements of steady-state response in V_m and Ca^{2+} at the same location were done sequentially and pacing signal was used to align beats, as previously reported[4]. Fluorescence signals were recorded with a photomultiplier tube at a fixed distance (1.2-1.6cm) from the electrode at a sampling rate of 1kHz. After achieving steady state by pacing for 60 beats 20 transients in the voltage and then the calcium domain were collected. Using an automatic pacing protocol and filter switch, cells were paced up through failure to follow 1:1 (occurrence of alternans or conduction block), and then down, decreasing pacing frequency. At each frequency step, V_m and Ca^{2+} signals were acquired at steady-state. Hysteresis was measured as the difference between the frequency of appearance of alternans upon increase in frequency minus the frequency of disappearance of alternans while decreasing frequency. **Suppl. Fig. 3** summarizes the results.

Ultra-high resolution optical mapping of intracellular calcium

Ca^{2+} measurements were performed 4–6 days after culture in an experimental chamber perfused with oxygenated Tyrode solution (in mM: 1.33 CaCl2, 5 glucose, 5 HEPES, 1 MgCl2, 5.4 KCl, 135 NaCl, and 0.33 NaH2PO4, with pH adjusted to 7.4 using NaOH) at 30 ± 1°C. Cells were stained with the Ca^{2+}-sensitive dye fluo 4 (8 µM; Molecular Probes) at room temperature for 20 min, and unincorporated stain was washed out for another 20 min.

We applied ultra-high-resolution imaging with an intensified CMOS camera (1280 × 1024 pixels, pco camera) and Video Scope Gen III intensifier coupled to a high NA lens (Navitar Platinum, f/1). The field of view (FOV) was approximately 2.2x2.2cm; spatial resolution after 2x2 binning was (44x44µm in x-y); temporal resolution was 200 fps. The system is able to achieve cell-level resolution over a very large FOV.

All experiments were conducted while samples were perfused with Tyrode's solution at 30^{o}C. Pacing was applied via platinum line electrodes on one side of each sample. Cardiomyocytes are paced following a programmed pacing protocol with a total duration of around 10 minutes: starting at 1 Hz with a step of 0.5Hz, and then from 2Hz to 7.5Hz with a step of 0.2Hz. For each pacing frequency, the acquisition system is programmed to pause for 30 beats without recording so that steady-state is reached, followed by a record of 30 beats before switching to the next pacing frequency.

Data processing

Pre-processing of the optical mapping recordings (typically 5 gigabytes per record) was done using advanced signal and image-processing methods and custom-designed software in Matlab (MathWorks, Natick, MA). Signal filtering included temporal Savitzky-Golay filter (2nd order, 7 frame window) and a spatial 3x3 Bartlett filter. Automatic beat detection was applied after baseline subtraction and enhancement of contrast. Further automated detection of peak height of calcium transients, calcium transient duration (CTD), rise time and other morphological paramaters was done for all spatial locations (pixels) over all beats to form 3D data sets.

Activation maps were constructed by contour plots of the automatically detected time of activation. Conduction velocity (CV) was calculated from quasi-1D samples (18x2mm) by a least square linear fit over the spatiotemporal plot along all pixels versus their corresponding activation time for individual beats. For a subset of samples, we quantified wavefront fractionation to assess the uniformity of uncoupling by heptanol. Wavefront fractionation was measured (in μm) as follows (see **Suppl. Fig. 4**):

$$\frac{norm(d,2)}{n} = \frac{\sqrt{\sum_{i=1}^{n} d_i^2}}{n} \qquad (5)$$

where d_i represents the Euclidean distance of an actual point (of certain activation time) from the fitted wavefront (isochrone) with that activation time; n is the number of points for a given wavefront.

Ca^{2+} alternans were detected and stored with preservation of phase using a recently published algorithm[10], which is the first to our knowledge that provides reliable alternans detection in conditions of low signal-to-noise ratio, such as occurring at extremely fine spatial scale and for very small amplitude alternans (at the detection limit). And it was essential for capture of early fine-scale Ca^{2+} alternation in this study.

In detail, we use an index of temporal persistence (TP) of alternating signals as the basis of our algorithm for automatic alternans detection. TP is defined as the ratio between the longest length of a segment of uninterrupted alternans and the total signal length (number of beats). From the original traces a representative signal parameter is extracted, e.g. peak height of calcium concentration. Then derivative and sign are taken along the time dimension to accentuate the alternating patterns and the signal is binarized. Interruptions in alternating patterns are found by locating the zeros after another derivative to calculate the longest length of an uninterrupted alternating. Furthermore, based on the TP concept, we introduce representative phase (RP) derived in time-overlapping segments for different spatial locations to help identify spatially discordant alternans (SDAs); RP assumes values of -1 or +1, and is used in conjunction with the calculated alternans rato (AR), defined as $\left|1 - A_{odd} / A_{even}\right| * 100,\%$, where the amplitude of the calcium transients at odd and even beats is used.

Random noise is likely to display beat-to-beat alternation and to exhibit some level of temporal persistence in such patterns. For example, for a random binary sequence of length 30 this likelihood is TP≈23%. TP of noise varies with signal length. Therefore, to distinguish with sufficient confidence alternans from noise, a threshold level (minimum TP of detection) must be chosen sufficiently higher than TP seen in white noise.

For a subset of samples, we applied a spatial clustering analysis based on detected alternans phase. We used k-means cluster algorithm, implemented in Matlab (MathWorks). It partitions points into k clusters by using a two-phase iterative algorithm to minimize the sum of point-to-centroid distances. Where applicable, normality of distribution for the groups was confirmed using the Lilliefors test. Statistical analysis was done using ANOVA with post-hoc Tukey-Kramer correction for multiple comparisons.

Power analysis was applied to the CTD80 data using bootstrapping simulations and a non-parametric test. More specifically, bootrstapping (in Matlab) was used to run simulations with different sample size, i.e. sample size was increased using the original samples for the 4 groups, then 2x, 3x and 4x the original size. For each case, 1000 simulations per group were run using bootstrapping. A non-parametric (Kruskal-Wallis) test was applied to check for differences between groups in these simulations. The percentage of cases/simulations that passed the significance test was used to determine the power at that sample size. In addition, the detectable change was determined for each case based on simulations for which significance was achieved.

Correlation analysis for CTD effects (testing for correlation between CTD80 and areas of early alternans) was done using several different approaches, including the Kendall tau rank test (**Suppl. Fig 5A**) on the pooled data from all groups, a non-parametric test for independence in two dimensions with chi-squared statistics applied to each of the four experimental groups, as well as visual trend/histogram representation (**Suppl. Fig 5B**).

Model simulations of diffusion using the classic diffusion equation

We first considered the classic diffusion equation for homogeneous isotropic two-dimensional medium:

$$\frac{\partial C}{\partial t} = D\left(\frac{\partial^2 C}{\partial x^2} + \frac{\partial^2 C}{\partial y^2}\right) \tag{6}$$

For initial conditions, where the local change in concentration is described by the Dirac function, the analytical solution is given by Crank[11] as follows:

$$C(r,t) = \frac{Co}{\left(2\sqrt{\pi Dt}\right)^n} \exp\left(-\frac{r^2}{4Dt}\right) \tag{7}$$

Parameters include distance, *r*, from the origin, time, *t*; factor n=2 for two-dimensional isotropic medium; C_o = 1 (concentration per area) is the initial concentration at $r = 0$, $t = 0$. The diffusion constant, D, was varied between 0.5 and 4.5 (area per time). An arbitrary concentration threshold of 0.0049 was imposed to illustrate the behavior of the model (**Suppl. Fig 2**).

Computer simulations of Ca^{2+} alternans and variable diffusion in a cardiac ionic model

We also modeled voltage and calcium dynamics in a two dimensional tissue using the reaction-diffusion equation:

$$\frac{\partial V}{\partial t} = -\frac{I_{ion}}{C_m} + D\left(\frac{\partial^2 V}{\partial x^2} + \frac{\partial^2 V}{\partial y^2}\right), \tag{8}$$

where C_m = 1 μF/cm^2 is the membrane capacitance, D is the effective diffusion coefficient of membrane voltage in cardiac tissue, and where I_{ion} is the total ionic current density. The reaction-diffusion equation was integrated with an operator splitting method, and adaptive time step method [12]. The space step was 0.015 cm and the time step varied from 0.1 to 0.01 ms. The ionic current was modeled by integrating a model of Ca^{2+} cycling of Shiferaw et al.[13], with the canine action potential model of Fox et al.[14]. Cellular alternans can be generated in this model either by a dynamical instability of V_m or by Ca^{2+} dynamics[15]. In our simulations model parameters were adjusted so that alternans were due to an instability in Ca^{2+} cycling dynamics via a steep release load relationship (see [15] for details). We modeled the case of electromechanically concordant alternans, in which a long APD is associated with a large Ca^{2+} transient, since this "positive coupling" scenario[15] agrees with the experimentally observed relationship between the Ca^{2+} transient and the APD in our neonatal rat culture (**Suppl. Fig 3**). The strength of the electromechanical (V_m-Ca^{2+}) coupling in the model was controlled by the time scale of recovery for L-type Ca^{2+} channel, where a very fast kinetics makes it insensitive to the previous diastolic interval and abolishes the feedback that APD alternans have on Ca^{2+} alternans.

In order to model the spatial evolution of alternans amplitude in tissue we considered a strip of cardiac tissue 150 cells long and 3 cells wide. Heterogeneous Ca^{2+} cycling properties were incorporated by adjusting cell model parameters in a region of size 20 by 3, in the center of the tissue, so that cells in this region were unstable to Ca^{2+} alternans at a pacing rate of 250ms, while cells outside this region were stable i.e. they did not display alternans when uncoupled from the tissue and paced at 4Hz. We then paced the tissue for 70 beats until steady state was reached, similar to the experiments. Spatial profiles of Ca^{2+} and APD alternans amplitude were then measured and plotted. This simulation was repeated with different values of the voltage diffusion coefficient in the range: D_v=0.24~1.8*10^{-3} cm^2/ms.

Computer simulations of Ca^{2+} alternans and variable diffusion using amplitude equations

In a more general way, the effect of voltage diffusion on the spatial distribution of Ca^{2+} alternans can be studied by deriving equations that govern the amplitudes of Ca^{2+} and APD alternans[16, 17], i.e. amplitude equations. This approach is applicable close to the period doubling bifurcation where the amplitudes of alternans are small and evolve slowly over many beats, and thus relevant to the case of early, fine-scale alternans examined here. We assume a one dimensional cable where each cell is paced simultaneously. The amplitude of APD and Ca^{2+} alternans at position x and time t are denoted as $a(x,t)$ and $c(x,t)$ respectively. The spatiotemporal evolution of small-amplitude alternans is then governed by a coupled system of partial differential equations:

$$\frac{\partial a}{\partial t} = \alpha\, a + \beta c - \Gamma_a a^3 + \xi_v \frac{\partial^2 a}{\partial x^2} \qquad (9)$$

$$\frac{\partial c}{\partial t} = \gamma\, a + \delta c - \Gamma_c c^3 + \xi_c \frac{\partial^2 c}{\partial x^2} \qquad (10)$$

The variables are described below:

i. The variables ξ_v and ξ_c represent the diffusive spread during a single paced beat of voltage and Ca^{2+}, respectively. In the amplitude equation formulation, these quantities are related to the diffusion coefficients of voltage and Ca^{2+} according to $\xi_v = \sqrt{D_v T}$ and $\xi_v = \sqrt{D_v T}$, where T is the pacing period and D_v and D_c are the diffusion coefficients of voltage and Ca^{2+}, respectively. Note that in cardiac tissue $\xi_v/\xi_c \gg 1$ since voltage diffuses much faster than Ca^{2+}. In this study we fix $T = 1$.

ii. The variable α denotes the growth rate of APD alternans. If $\alpha > 0$, then APD restitution is steep and the APD will alternate ($a > 0$) independently of Ca^{2+}. Here, we will assume that voltage is stable ($\alpha < 0$) and that Ca^{2+} cycling is the underlying nonlinearity for alternans. This assumption is justified by our observation of fine-scale alternans, as discussed in the main text.

iii. The variable δ denotes the growth rate of the Ca^{2+} cycling instability; $\delta > 0$ in this study to reflect that alternans are due to Ca^{2+} cycling.

iv. The parameters γ and β denote the coupling between APD alternans on Ca^{2+} alternans amplitude, and vice versa. Here we assume positive coupling (positive values for γ and β) based on observed electromechanical concordance in our system.

v. The variables Γ_a and Γ_c are constant parameters to ensure that alternans amplitudes stabilize at a finite value.

Using the system of equations above, we confirm our numerical findings with the full ionic model that an increase in ξ_v leads to a decrease in Ca^{2+} alternans amplitude, and that the area of tissue with Ca^{2+} alternans above a threshold value has a non-monotonic dependence on ξ_v. For the results shown in **Suppl. Fig 6**, we considered a cable of $N = 1000$ cells where the central 30 cells were unstable to Ca^{2+}. The parameters used in the model are: $\alpha = -0.1, \beta = 0.1, \gamma = 0.1, \Gamma_c = 0.01, \Gamma_v = 0, \xi_c = 0.5$. Ca^{2+} alternans is made unstable by setting $\delta = 0.01$ for the middle 30 cells, and $\delta = -0.1$ for the rest of the tissue. A threshold for the alternans amplitude is set at 1.2 to quantify the area.

References:

1. Entcheva E, Bien H. Tension development and nuclear eccentricity in topographically controlled cardiac syncytium. *Biomedical Microdevices*. 2003;5:163-168
2. Yin L, Bien H, Entcheva E. Scaffold topography alters intracellular calcium dynamics in cultured cardiomyocyte networks. *Am J Physiol Heart Circ Physiol*. 2004;287:H1276-H1285
3. Bien H, Yin L, Entcheva E. Calcium instabilities in mammalian cardiomyocyte networks. *Biophys.J.* 2006;90:2628-2640
4. Chung CY, Bien H, Entcheva E. The role of cardiac tissue alignment in modulating electrical function. *J Cardiovasc Electrophysiol*. 2007;18:1323-1329

5. Chung CY, Bien H, Sobie EA, Dasari V, McKinnon D, Rosati B, Entcheva E. Hypertrophic phenotype in cardiac cell assemblies solely by structural cues and ensuing self-organization. *Faseb J*. 2011;25:851-862
6. Jia Z, Gordon C, Bien H, Brink PR, Entcheva E. Anti-arrhythmic effects of 4-phenylbutyrate (4pb) in cardiac myocytes. *Circulation*. 2009;120:S653-S654
7. Wade MH, Trosko JE, Schindler M. A fluorescence photobleaching assay of gap junction-mediated communication between human cells. *Science*. 1986;232:525-528
8. Axelrod D, Koppel DE, Schlessinger J, Elson E, Webb WW. Mobility measurement by analysis of fluorescence photobleaching recovery kinetics. *Biophys J*. 1976;16:1055-1069
9. Soumpasis DM. Theoretical analysis of fluorescence photobleaching recovery experiments. *Biophys J*. 1983;41:95-97
10. Jia Z, Bien H, Entcheva E. Detecting space-time alternating biological signals close to the bifurcation point. *IEEE Trans Biomed Eng*. 2010;57:316-324
11. Crank J. *The mathematics of diffusion*. Oxford: Oxford University Press; 1975.
12. Qu Z, Garfinkel A. An advanced algorithm for solving partial differential equation in cardiac conduction. *IEEE Trans Biomed Eng*. 1999;46:1166-1168
13. Shiferaw Y, Watanabe MA, Garfinkel A, Weiss JN, Karma A. Model of intracellular calcium cycling in ventricular myocytes. *Biophys.J*. 2003;85:3666-3686
14. Fox JJ, McHarg JL, Gilmour RF, Jr. Ionic mechanism of electrical alternans. *Am J Physiol Heart Circ Physiol*. 2002;282:H516-H530
15. Shiferaw Y, Sato D, Karma A. Coupled dynamics of voltage and calcium in paced cardiac cells. *Phys Rev E Stat Nonlin Soft Matter Phys*. 2005;71:021903
16. Echebarria B, Karma A. Instability and spatiotemporal dynamics of alternans in paced cardiac tissue. *Phys Rev Lett*. 2002;88:208101
17. Shiferaw Y, Karma A. Turing instability mediated by voltage and calcium diffusion in paced cardiac cells. *Proc.Natl.Acad.Sci.U.S.A*. 2006;103:5670-5675

Supplementary Figure 1. Relative effects of heptanol on CV via suppression of Na^+ channels and suppression of gap junctions. Shown are two experimental dose-response curves. Left: Sigmoid curve fit to experimental data from Nelson & Makieski in dog Purkinjie cells on the effects of heptanol on Na^+ channel availability. Indicated is $k_{0.5}$ = 1.3mM, along with the low concentrations used in our study and the respective gNa levels based on this dose-response curve. Right: Sigmoid curve fit to experimental data from Brette & Orchard in adult rat cardiomyocytes on the effects of TTX on Na^+ channel availability. Indicated is $k_{0.5}$ = 0.75 μM, along with 4 TTX concentrations (red diamonds) used in our study to perturb gNa levels and measure CV. These data were used implicitly in **Fig 2c**.

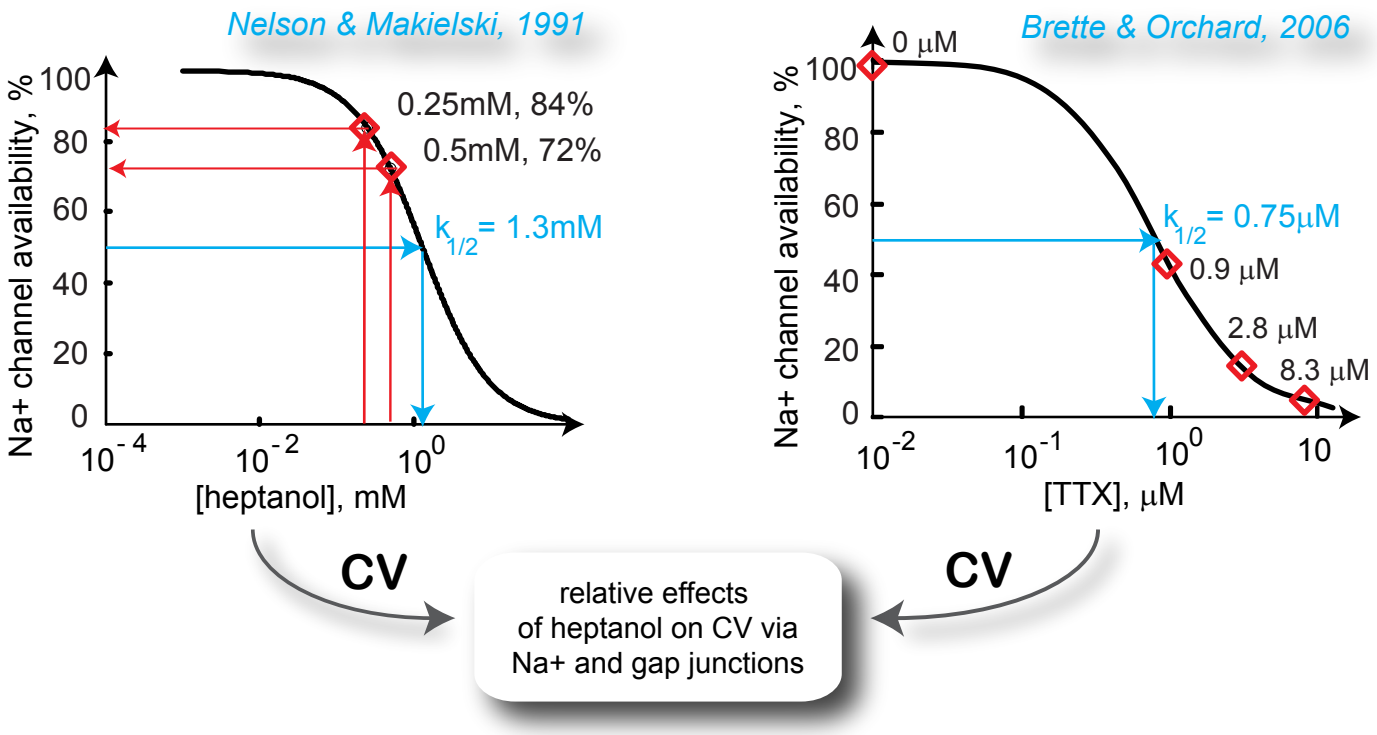
Nelson & Makielski, 1991
Na+ channel availability, %
100
80
60
40
20
0
0.25mM, 84%
0.5mM, 72%
k1/2= 1.3mM
10- 4
10- 2
100
[heptanol], mM
CV
relative effects
of heptanol on CV via
Na+ and gap junctions
CV
Brette & Orchard, 2006
0 μM
Na+ channel availability, %
100
80
60
40
20
0
k1/2= 0.75μM
0.9 μM
2.8 μM
8.3 μM
10-2
10-1
100
10
[TTX], μM

Supplementary Figure 2. Explanation of the effects of coupling on the spatial properties of Ca^{2+} alternans by considering diffusion + a threshold A. Using an analytical solution of the generic diffusion equation for two-dimensional medium and a Dirac function of concentration change as initial condition, we obtain the spatial profiles at a fixed time for different degrees of coupling. **B.** Quantification of spatial patterns (from **A**) by imposing a threshold (left); average concentration after a fixed time as function of diffusion properties (middle); area of concentration above a threshold as function of diffusion properties (right). Compare **B**-middle to **Fig 4D**, and **B**-right to **Fig 4E&F**.

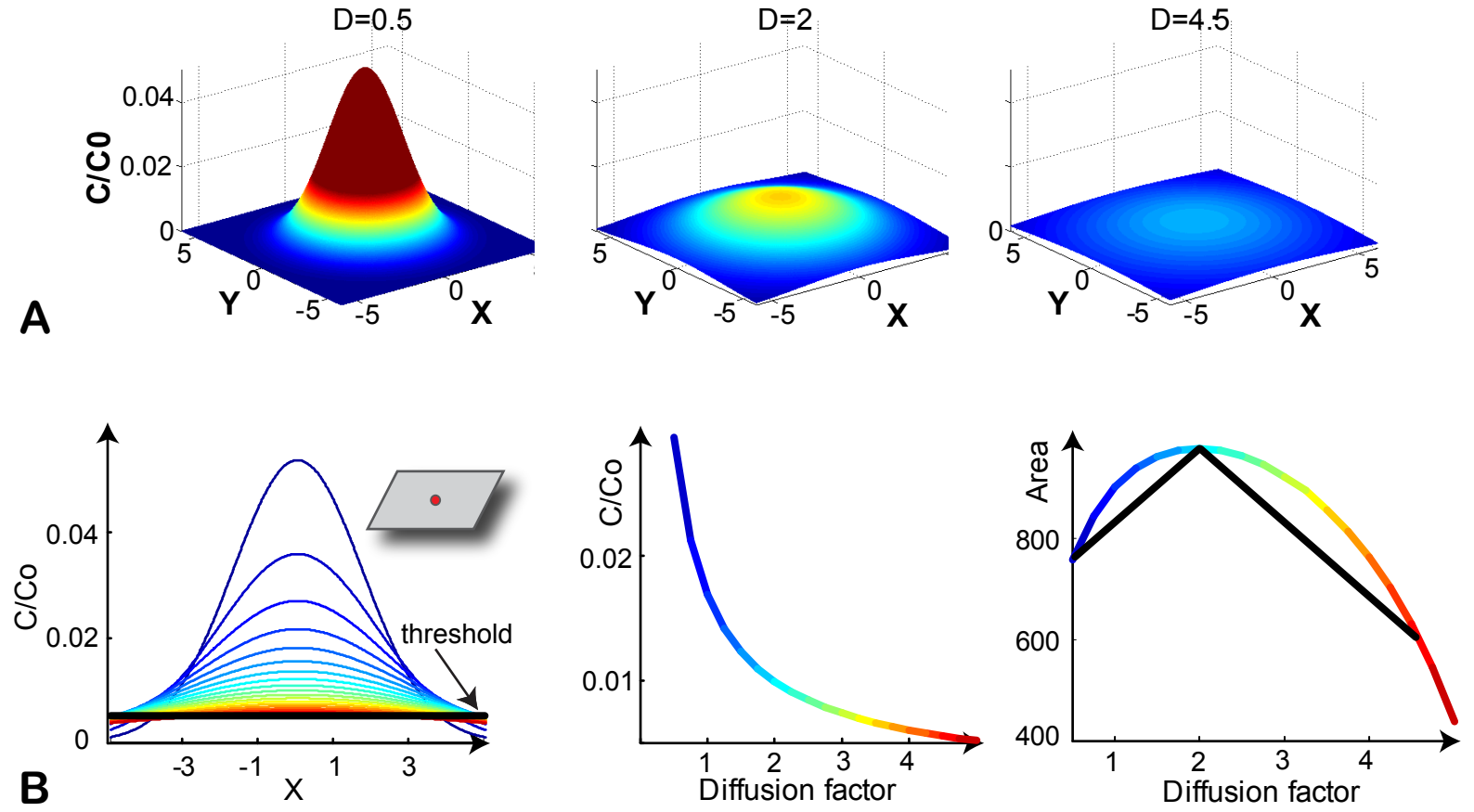
A
D=0.5
D=2
D=4.5
C/C0
0.04
0.02
0
5
0
-5
Y
X
B
C/Co
threshold
-3
-1
1
3
Diffusion factor
Area
800
600
400

Supplementary Figure 3. Experimental evidence for strong positive V_m-Ca^{2+} coupling and electromechanical concordance A. Representative traces of voltage and Ca^{2+} from the same sample at different frequencies during 1:1 response, alternans (2:2) and blocks (2:1). Scale bar is 1s. **B.** Quantitative analysis of memory (hysteresis) in the induction and disappearance of V_m and Ca^{2+} alternans (n = 16). Samples were paced progressively towards higher frequencies until appearance of alternans (fa) and then back towards slower rates to determine the frequency of disappearance (fd), see bottom inset. Hysteresis was quantified as (fa – fd). Data for all 16 samples are shown as a scatter plot, and as a bar graph (top inset) with mean±S.D.

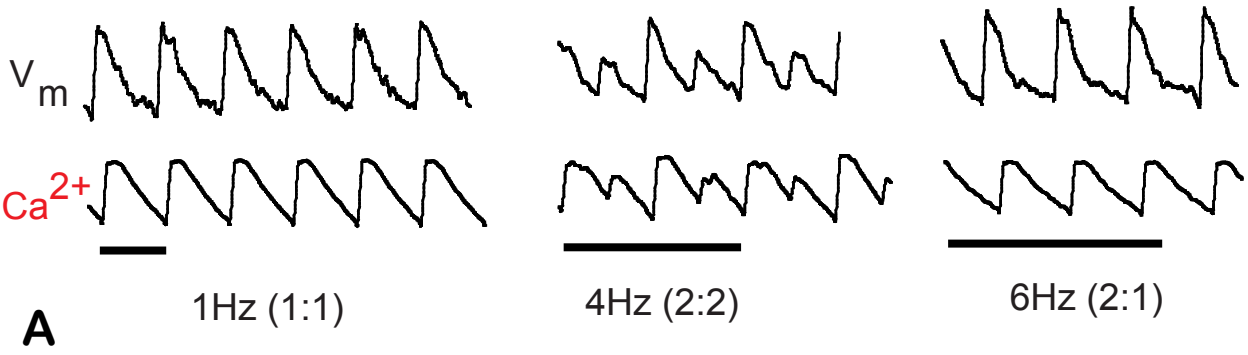
Vm
Ca2+
1Hz (1:1)
4Hz (2:2)
6Hz (2:1)

A

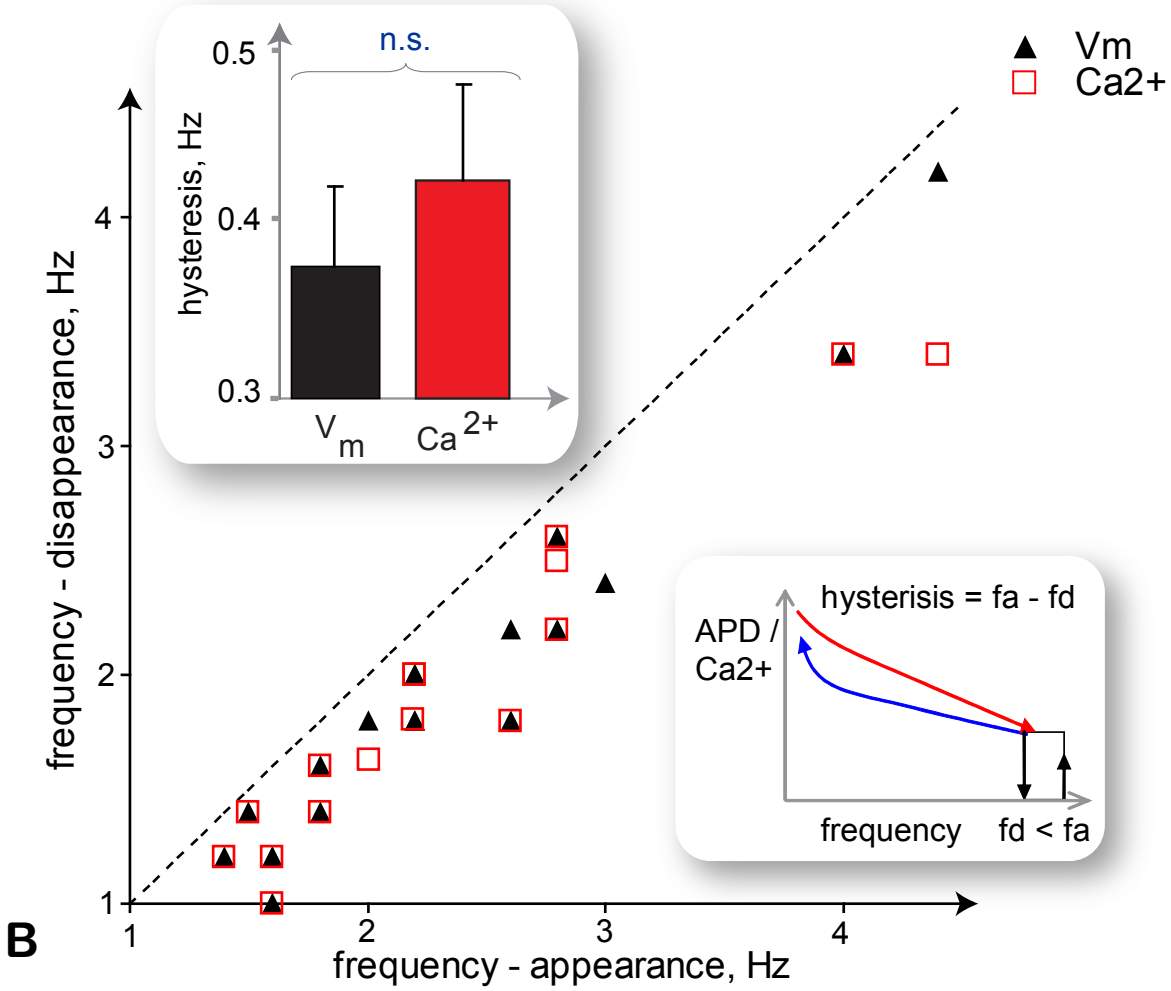
Vm
Ca2+
n.s.
0.5
0.4
0.3
hysteresis, Hz
Vm
Ca2+
hysterisis = fa - fd
APD /
Ca2+
frequency
fd < fa
frequency - disappearance, Hz
frequency - appearance, Hz
1
2
3
4

B

Supplementary Figure 4. Assessing wavefront fractionation upon uncoupling with low doses of heptanol. A. An example wavefront with a fitted curve (isochrone) and the actual points having the same activation time. **B.** Calculation of residuals and norm for the shown example. **C.** Summary of results for wavefront fractionation (norm/N, where N is the number of points in the wavefront) for control, 0.25 mM and 0.5 mM heptanol treated; number of samples indicated, mean±SEM.

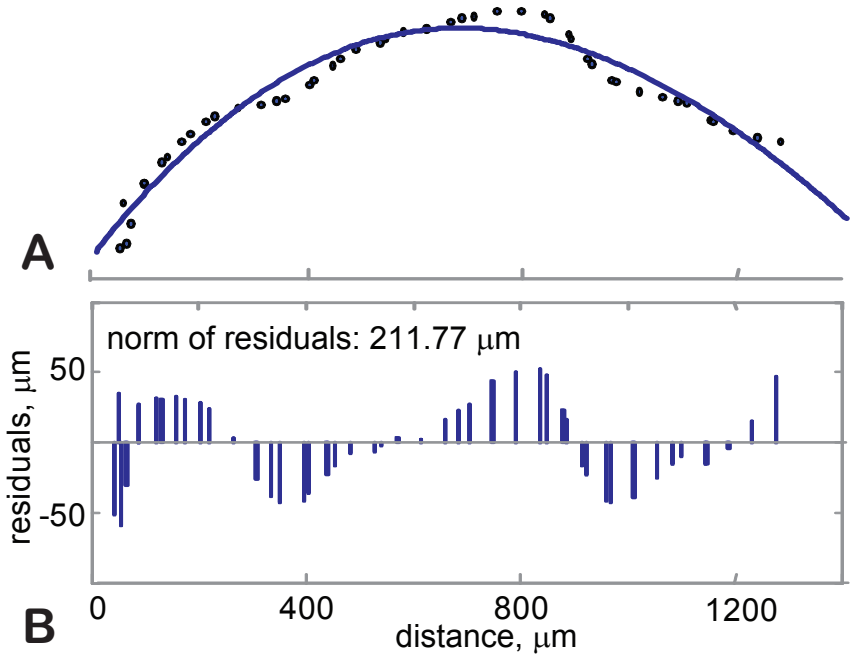
A
norm of residuals: 211.77 μm
residuals, μm
50
-50
0
400
800
1200
distance, μm
B

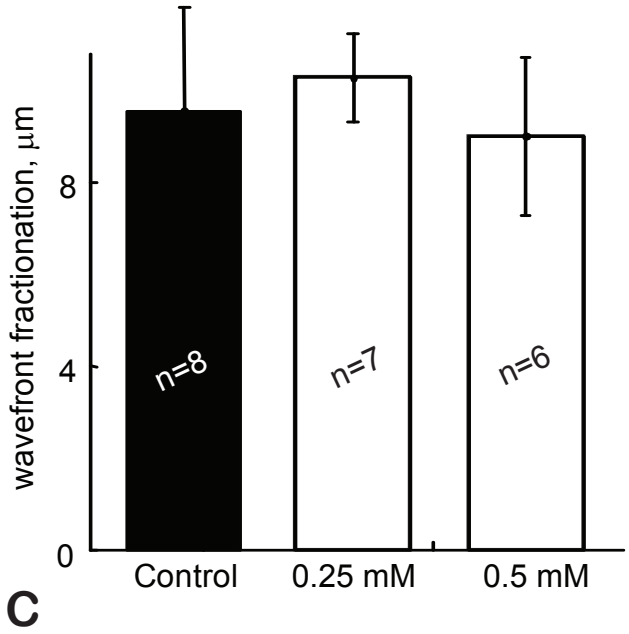
wavefront fractionation, μm
8
4
0
n=8
n=7
n=6
Control
0.25 mM
0.5 mM
C

Supplementary Figure 5. Lack of significant correlation between the CTD80 and early (pre-threshold) areas of alternation. A. Pooled data from all four groups are shown in a scatter plot; Kendall tau rank correlation test yields correlation coefficient r=0.07 (at p=0.51). **B**. Trend/histogram analysis of the CTD80 and fine alternans area per group; data are binned in 0.05 s and 0.5%, respectively. A non-parametric test for independence of two dimensions applied to each group further corroborated lack of significant correlation - χ^2 and p-value for independence were as follows: (182, 0.23) for 4PB, (506, 0.24) for control, (182, 0.23) for 0.25mM heptanol, and (272, 0.24) for 0.5mM heptanol.

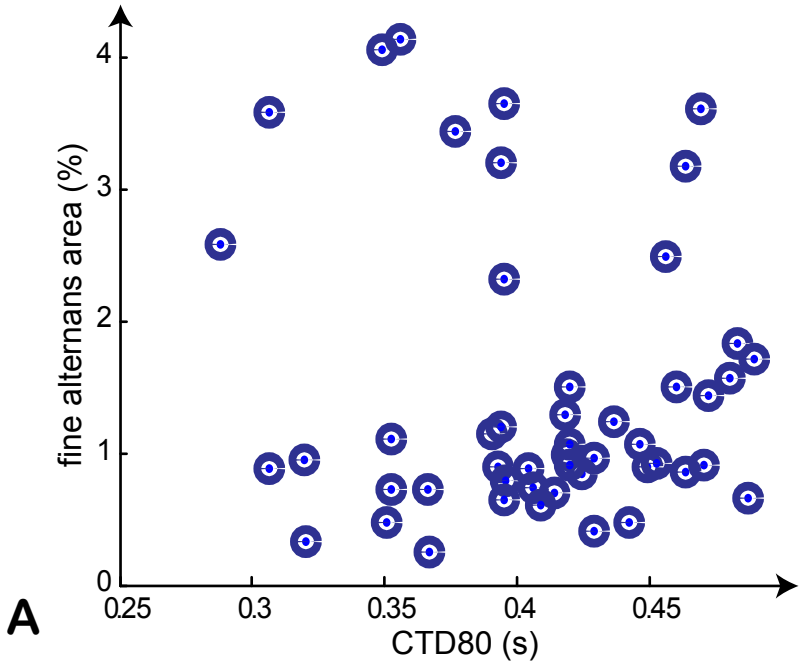
fine alternans area (%)
CTD80 (s)
0
1
2
3
4
0.25
0.3
0.35
0.4
0.45

A

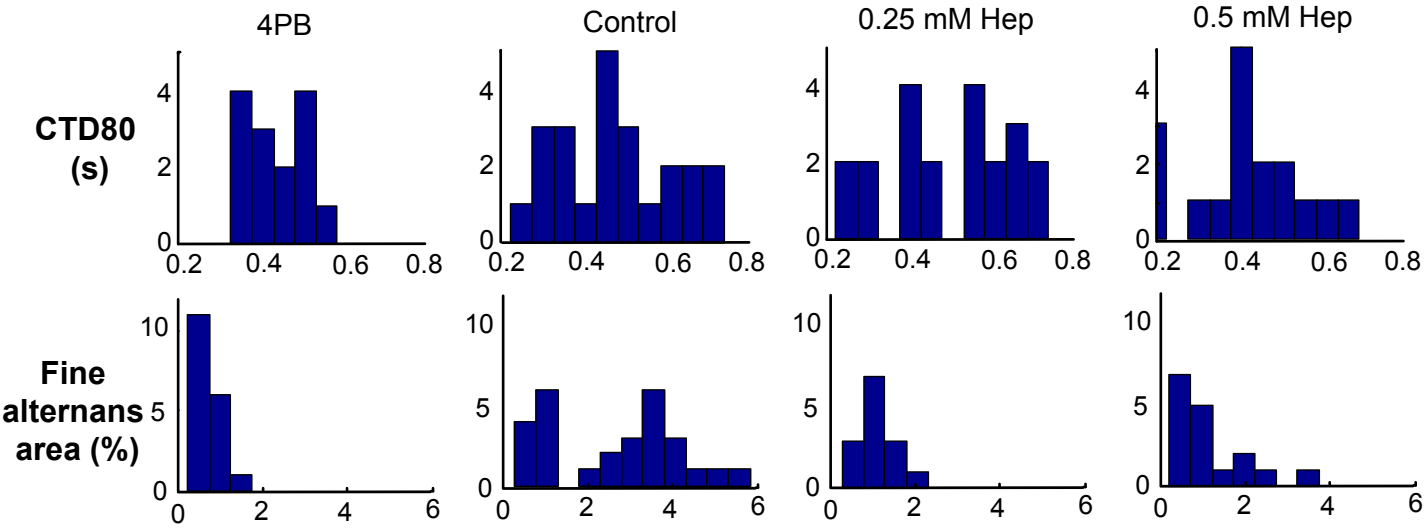
4PB
Control
0.25 mM Hep
0.5 mM Hep
CTD80 (s)
Fine alternans area (%)

B

Supplementary Figure 6. Using the amplitude equation to simulate the effects of coupling on the spatial properties of Ca^{2+} alternans. A. Amplitude of calcium alternans, c_p, as function of the effective diffusion coefficient for voltage, ξ_v. Compare to experimental results in **Fig 4D**, and model results in **Fig 5B** and **Suppl. Fig 2B**. **B.** Quantification of the area of local alternation (above a threshold of 1.2) as function of the effective diffusion factor, ξ_v. Compare to experimental results in **Fig 4E-F**, and model results in **Fig 5C** and **Suppl. Fig 2B**.

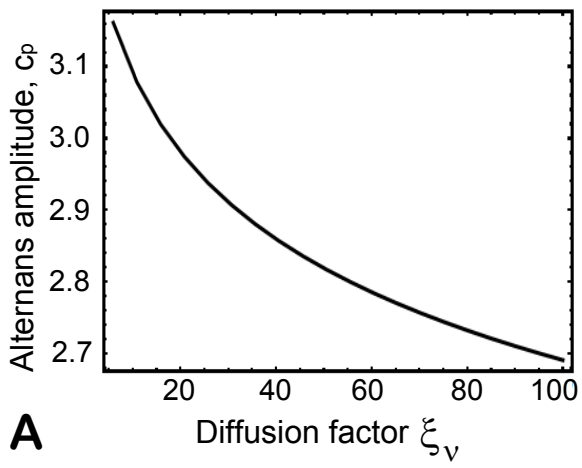
Alternans amplitude, c_p
3.1
3.0
2.9
2.8
2.7
20
40
60
80
100
Diffusion factor ξ_ν

A

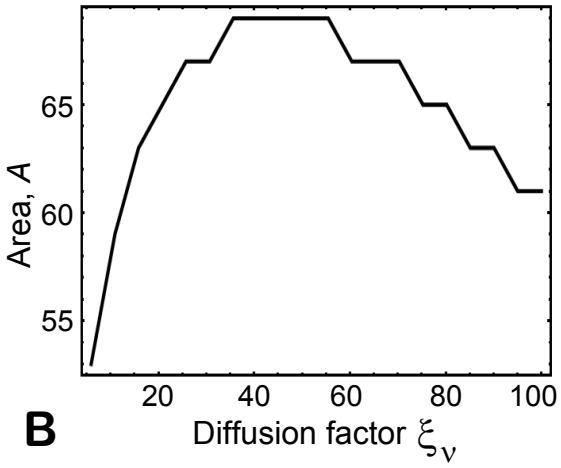
Area, A
65
60
55
20
40
60
80
100
Diffusion factor ξ_ν

B

Supplementary Figure 7. Predictive potential of the early fine-scale Ca^{2+} alternans in conjunction with coupling for later arrhythmia development. A. cellular coupling is linearly related to break-point frequency. **B.** The area of early fine Ca^{2+} alternans (<2Hz pacing) correlates significantly with the maximum alternans area upon break-point frequency. **C.** K-means cluster analysis applied to fine Ca2+ alternans at 2Hz pacing considering their phases successfully predicts the nodal line position developed at 4Hz pacing in the same sample.

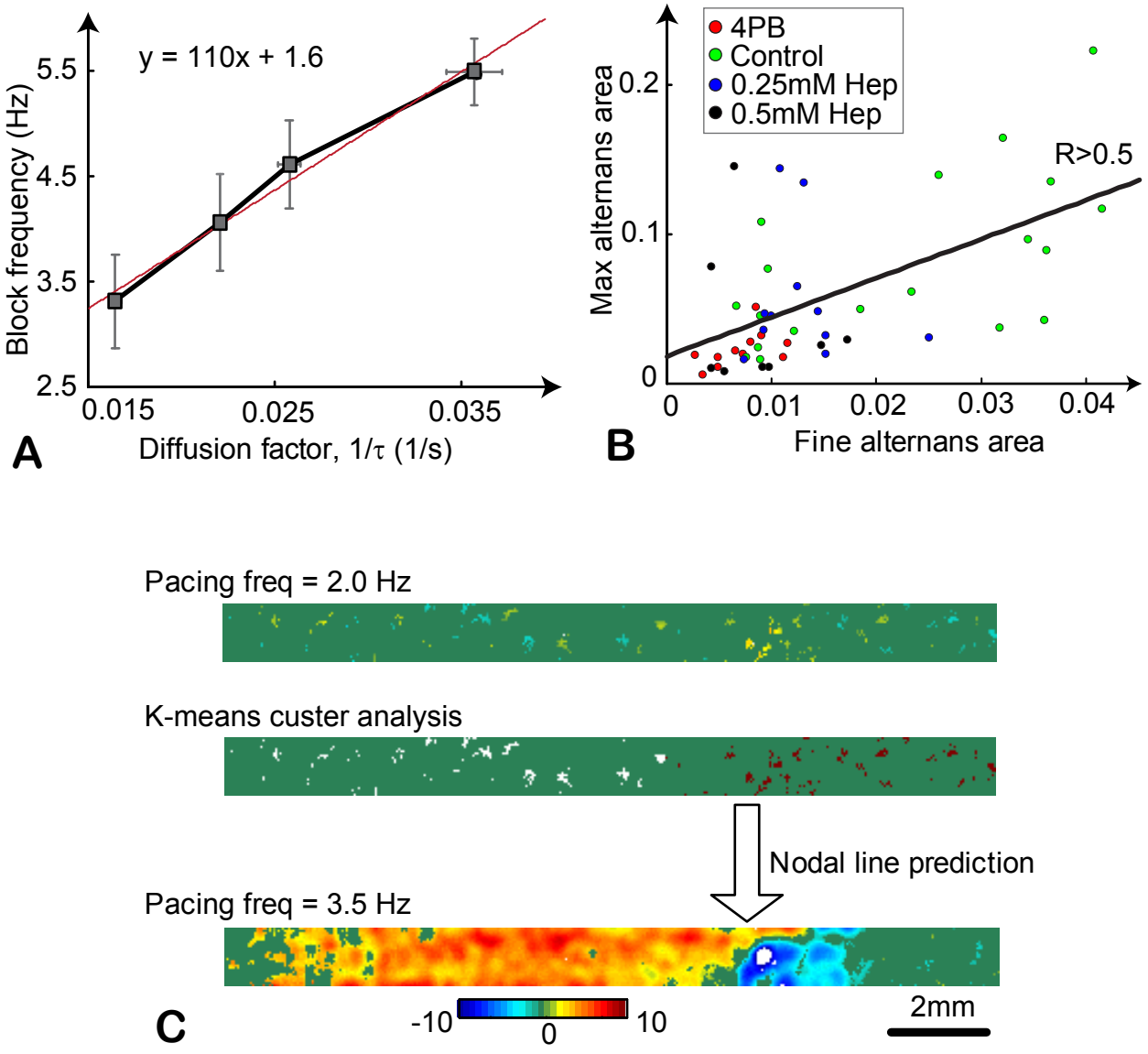
y = 110x + 1.6
Block frequency (Hz)
5.5
4.5
3.5
2.5
0.015
0.025
0.035
Diffusion factor, 1/τ (1/s)
A
4PB
Control
0.25mM Hep
0.5mM Hep
R>0.5
Max alternans area
0.2
0.1
0
0
0.01
0.02
0.03
0.04
Fine alternans area
B
Pacing freq = 2.0 Hz
K-means custer analysis
Nodal line prediction
Pacing freq = 3.5 Hz
-10
0
10
2mm
C